Optics Letters

Encoding and display with stereo split-ring resonator arrays

Zheng-Han Wang,[1] Yuan-Sheng Hu,[1] Xiang Xiong,[1,2] Ru-Wen Peng,[1,3] and Mu Wang[1,4]

[1]National Laboratory of Solid State Microstructures and School of Physics, Collaborative Innovation Center of Advanced Microstructures, Nanjing University, Nanjing 210093, China
[2]e-mail: xiang@nju.edu.cn
[3]e-mail: rwpeng@nju.edu.cn
[4]e-mail: muwang@nju.edu.cn

Received 28 December 2016; revised 8 February 2017; accepted 15 February 2017; posted 15 February 2017 (Doc. ID 283733); published 13 March 2017

In this Letter, we report on encoding and display based on stereo standing U-shaped resonator (SUSR) arrays. The SUSR serves as a perfect absorber at a structure-dependent frequency when the polarization of incident light is parallel to the bottom rim of the SUSR. When the incidence polarization is rotated for 90° (perpendicular to the bottom rim of the SUSR), the SUSR turns to a perfect reflector at broadband frequencies. Further, the resonant frequency sensitively depends on the height of the arms of the SUSR. By introducing SUSRs with different arm heights, a resonant absorption state may occur at different frequencies. By defining the resonant absorption state as "dark" and the reflection state as "bright," we can encode and display binary patterns. Beside, when the SUSR rotates with the direction of the standing arms as axis, a different reflectivity, hence, a different shade will be generated. In this way, we may realize a grayscale display. Experimentally, we demonstrate that this encoding and display scheme indeed works.

OCIS codes: (160.3918) Metamaterials; (120.2040) Displays; (220.4241) Nanostructure fabrication.

https://doi.org/10.1364/OL.42.001153

The history of manufactured mirror can be traced back to thousands of years ago [1]. Yet people never imagined that the same object can be used as a reflector (mirror) and an absorber by simply rotating its geometrical orientation. In recent decades, with the development of subwavelength optics and plasmonics, optical properties of a structured metal film have become extremely diverse [2–6]. These properties depend not only on the chemical composition of the material, but also on the subwavelength structural design. For example, conventional Snell's law describes the relationship between the angles of incidence and the refraction/reflection of a wave on a homogeneous boundary between two different isotropic media [7]. If, however, by introducing a two-dimensional array of resonators with a spatially varying phase response and a subwavelength separation on the interface (so the surface is called metasurface) [8–15], propagation direction of the refractive/reflective waves will carry the additional phase gradient induced by the artificial resonators on the interface. This effect may generate unprecedented applications in manipulating propagation directions of waves. The other unique properties induced by the strong interaction of the wave with the subwavelength structures include extraordinary transmission [16,17], giant optical activity [18–20], perfect absorption [5,21], and ultrahigh spatial resolution [22–26].

Despite the great achievements in applying metasurfaces, a three-dimensional (3D) metastructure offers additional flexibility in tuning the physical properties compared to its two-dimensional (2D) counterpart [6,27–31]. An apparent example is that the 3D metastructures may carry more information in encoding and display compared to the 2D metasurface. However, with a traditional top-down microlithography approach, fabricating 3D metastructures with complicated topography is a formidable task. In this Letter, we report on the design and fabrication of a series of standing U-shaped resonators (SUSRs) with two-photon absorption (TPA) process. The orientations of the bottom rim of the SUSR and the height of the standing arms of the SUSRs are used as control parameters for binary and grayscale encoding and display. We also fabricate the samples and demonstrate that this encoding and display scheme really works.

Previously, we have demonstrated that 3D SUSRs may work as polarization-dependent absorbers [6]. The arm height of the SUSR is a major factor to tune the absorption frequency. First, we utilize 3D SUSRs to construct pixels for a binary display. As shown in Fig. 1(a), the SUSRs are fabricated on a glass substrate, followed by metallization via coating the SUSR array and the glass substrate with continuous gold thin film. As illustrated in Fig. 1(a), the opening of the SUSR points to $+z$, and the incident light propagates in $-z$. The transmission and reflection spectra for the polarized incidence in Fig. 1(b) is calculated by the finite difference time domain method. [32] At a frequency of 1220 cm^{-1}, for x-polarized incidence, the SUSRs act as perfect absorbers, and the incident light neither transmits nor reflects from the surface. When the polarization of the

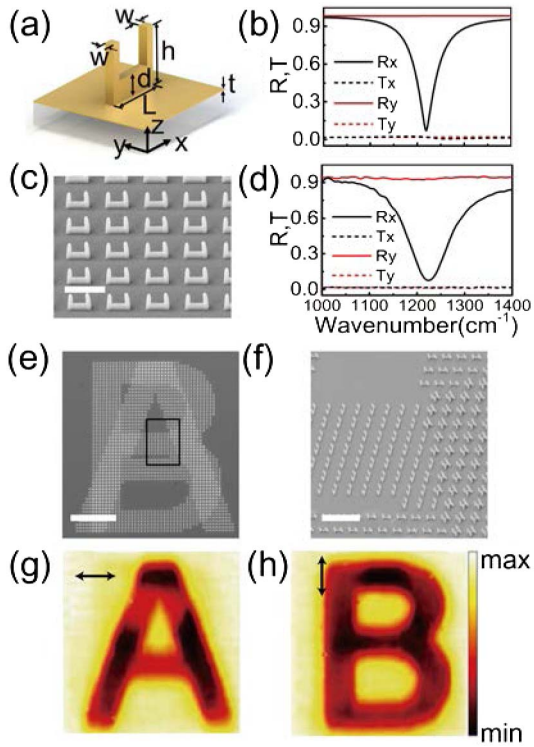

Fig. 1. (a) Schematic diagram of the designed SUSR unit, where $w = 0.3$ μm, $L = 2$ μm, $d = 0.7$ μm, $h = 1.9$ μm, and $t = 35$ nm. The lattice constant of the SUSR array is 4 μm. (b) R_x, R_y, T_x, and T_y are the simulated reflection and transmission coefficients of x- and y-polarization, respectively. (c) SEM micrograph of the fabricated SUSR array. The scale bar represents 4 μm. (d) Measured reflection and transmission spectrum of SUSR arrays. (e) SEM micrograph of the designed two letters "A" and "B." The scale bar represents 60 μm. (f) 45° tilted-angle view of the boxed region in (e). The scale bar in (f) represents 10 μm. (g) and (h) Measured FPA images for x- and y-polarization of incident light, respectively.

incident light is rotated for 90° (y-polarized), the incident light is perfectly reflected, similar to what happens on a mirror. We fabricate such a SUSR array via a TPA approach, where the focus point of an excimer laser scans a 3D pattern. The precursors in the regions scanned by the focus point are polymerized and solidified, whereas those in the rest of the regions are washed away by propylene glycol monomethyl ether acetate (Sigma-Aldrich). In this way, a polymer skeleton of SUSRs is fabricated. We then coat the polymer skeleton (and the glass substrate as well) with a gold film 35 nm in thickness by magnetron sputtering. The scanning electron micrograph (SEM, LEO 1530VP) of the structure is illustrated in Fig. 1(c). A Fourier transform infrared spectrometer (FTIR, Bruker Vertex v70) associated with an infrared microscope with a focal plane array detector (Bruker Hyperion 3000) is applied for optical characterization. The measured transmission and reflection spectra in Fig. 1(d) confirm that for x-polarized incidence, nearly zero reflection is achieved at 1220 cm^{-1}, whereas for y-polarized incidence, the incidence is perfectly reflected over a broad frequency range (1000–1500 cm^{-1}). Besides, our simulation shows that the SUSR still works as a polarization-sensitive absorber under oblique incidence. If the incident angle is less than 40°, the SUSR works well for both transverse electric (TE) and transverse magnetic (TM) modes. This could be useful for applications in active display devices, information storage, and encryption technology.

Herewith, we use the properties shown in Figs. 1(a)–1(d) to encode a pattern. We define the perfect reflection and perfect absorption as "bright" and "dark" states, respectively. Based on the orientation of the bottom rim of the SUSR and the polarization of the incident light, we define three types of pixels for binary display: $P(h, 0)$ represents dark in x-polarized incidence and bright in y-polarized incidence with the bottom rim of the SUSR in x-direction; $P(0, h)$ represents bright in x-polarized incidence and dark in y-polarized incidence with the bottom rim of the SUSR in the y-direction; and $P(h, h)$ represents dark in both x- and y-polarized incidence by combining two orthogonal SUSRs to form a fish-spear-like resonator (FSR). Two letters "A" and "B" are encoded with the SUSRs with different orientations to form a matrix 240 μm × 240 μm in size, as shown in Fig. 1(e). The structure is fabricated by TPA processing. As illustrated in Fig. 1(f), the overlap area of "A" and "B" is constructed with pixel $P(h, h)$, the rest of "A" is constructed with pixel $P(h, 0)$, and the rest of "B" is constructed with pixel $P(0, h)$. Different patterns can be displayed by switching the incidence polarization from x-polarized to y-polarized. Figures 1(g) and 1(h) show the images collected by the focal plane array detector. In the measurement, a ZnSe polarizer is applied to select the incident polarization. The reflection signals are integrated in the frequency range of 1200–1300 cm^{-1}. Letters "A" and "B" can be clearly identified when the incident light is set as x-polarized and y-polarized, respectively.

As shown in Fig. 1, we have experimentally proved that the reflection intensity of the SUSR unit is polarization sensitive. Further, the absorption frequency can be accurately tuned by changing the arm height of the SUSR unit. We can create pixels based on a FSR unit consisting of two orthogonal SUSRs, as shown in Fig. 2(a). The arm heights in each SUSR are h_1 and h_2, suggesting different absorption frequencies in two orthogonal polarization directions. We fabricate the FSR arrays with $h_1 = 1.8$ μm and $h_2 = 2.3$ μm, as illustrated in Fig. 2(b). The measured FTIR spectra in Fig. 2(c) indicate that by setting different arm heights of the orthogonal SUSRs, indeed the absorption frequencies can be independently tuned for the two orthogonal polarizations directions.

To display a binary image, four types of pixels with different h_1 and h_2 heights are designed: $P_{(hi,hj)}$ stands for the scenario that within a FSR unit the height of the SUSR in x- and y-direction s is h_i and h_j, respectively. In this design, h_1 is taken as 1.8 μm, and h_2 is taken as 2.3 μm. Two letters "C" and "D" are encoded with FSR pixels in this way: the area where "C" and "D" overlap is constructed with pixels of type $P_{(h1,h1)}$ the rest of "C" and the rest of "D" are constructed with pixels of $P_{(h1,h2)}$ and $P_{(h2,h1)}$, respectively. The blank area that displays neither a "C" nor a "D" pattern is constructed with pixels of $P_{(h2,h2)}$. The morphology of the fabricated sample is shown in Fig. 2(d). By illuminating the sample with x- and y-polarized incident light and integrating the reflection signals in 1220–1320 cm^{-1}, the patterns "C" and "D" are displayed, respectively, as shown in Figs. 2(e) and 2(f).

It is possible to encode independently not only with different incident polarizations, but also at different frequencies. As shown in Fig. 3(a), we design a combo pixel constructed with

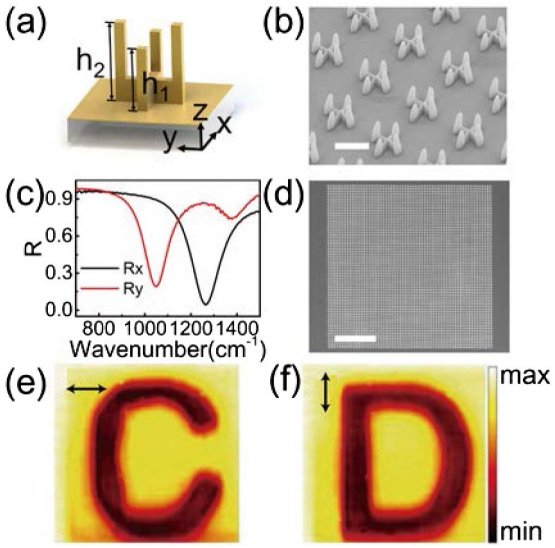

Fig. 2. (a) Schematic diagram of the pixel of the FFR unit. (b) SEM micrograph of 45° tilted-angle view of the FFR arrays, where $h_1 = 1.8$ μm and $h_2 = 2.3$ μm. The scale bar represents 2 μm. (c) Measured reflection spectrum of FFR arrays for incidence with different polarization states. (d) Morphology of the fabricated sample with two encoded letters "C" and "D." The scale bar represents 60 μm. (e) and (f) FPA images for *x*- and *y*-polarization of incidence, respectively.

four separated SUSRs. Figure 3(b) shows the top view of the pixel. Four SUSRs are placed end to end, forming a square. The staggered arrangement could weaken the coupling between the resonators. Each SUSR works as an independent channel within one combo pixel. Four independent channels are defined as follows: CH_1 and CH_3 work in *x*-direction polarization, and their bottom rims are in parallel to the *x*-direction CH_2 and CH_4 work in *y*-direction polarization, and their bottom rims are in parallel to the *y*-direction; CH_1 resonates for *x*-polarized incidence at 1045 cm^{-1}, CH_2 resonates for *y*-polarized incidence at 1045 cm^{-1}, CH_3 resonates for *x*-polarized incidence at 1220 cm^{-1}, and CH_4 resonates for *y*-polarized incidence at 1220 cm^{-1}. When the arm height of CH_1 and CH_2 is set as 2.3 μm, both CH_1 and CH_2 act as absorber and are defined as "dark." The height of CH_3 and CH_4 is set as 1.9 μm to achieve the "dark" state at 1220 cm^{-1}. Similarly, we can define "bright" states for all channels by setting the SUSR height as 1.5 μm, which possesses resonant absorption at 1520 cm^{-1} and reflects perfectly at both 1220 and 1045 cm^{-1}. Figures 3(c) and 3(d) show the SEM micrograph of the fabricated sample made of the combo pixels. Four letters "E", "F", "G," and "H" have been encoded with CH_1, CH_2, CH_3, and CH_4, separately. With the FPA imaging technique, "E" is displayed in CH_1 by integrating the reflecting signals at 1045cm^{-1} with *x*-polarized illumination, as shown in Fig. 3(e). Similarly, "F" is displayed in CH_2 at 1045 cm^{-1} with *y*-polarized illumination. "G" and "H" appear in CH_3 at 1220 cm^{-1} with *x*-polarized illumination and in CH_4 at 1220 cm^{-1} with *y*-polarized illumination, respectively. It should be noted that the two reflection dips collected along the same polarization have some overlap in frequency range, which slightly decreases the contrast of the image.

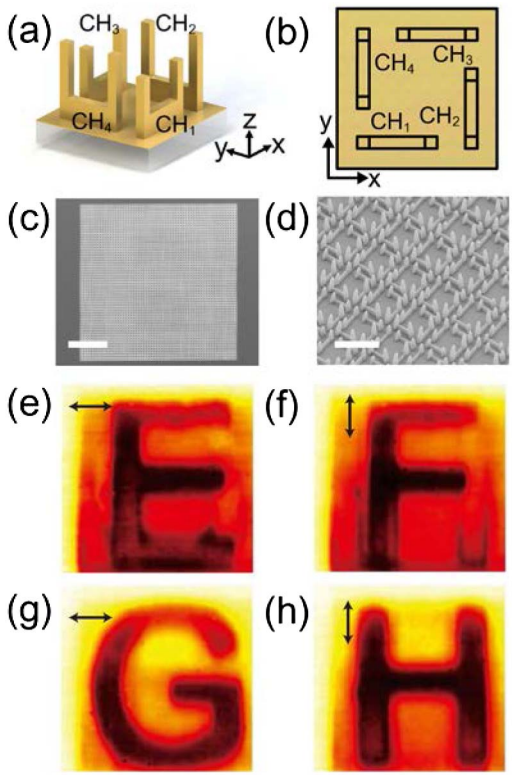

Fig. 3. (a) Schematic diagram of the combo pixel made of four SUSRs. (b) Top view of the combo pixel unit. (c) and (d) show the SEM micrographs of the fabricated sample. The scale bar in (c) represents 60 μm, and the scale bar in (d) represents 4 μm. (e) and (f) show the FPA images integrated in 1000–1100 cm^{-1} for *x*- and *y*-polarized incidence, respectively. (g) and (h) show the FPA images integrated in 1200–1300 cm^{-1} for *x*- and *y*-polarized incidence, respectively.

We develop further an approach to display grayscale images with SUSR pixels. As illustrated in Fig. 4(a), θ describes the angle between the bottom rim of the SUSR and the *x*-axis. At the absorption frequency, the reflection intensity can be expressed as

$$R_\theta = 1 - A_0 \cos^2(\theta), \quad \textbf{(1)}$$

where A_0 is the maximum absorbance when the SUSR is parallel to the *x*-direction. Figure 4(b) demonstrates the simulation of reflection R_θ with respect to θ. When the incidence polarization is fixed, the reflection strength of each pixel can be selected by choosing the rotating angle θ of each SUSR pixel. Figure 4(c) shows a picture that works as a source image in the grayscale display. The key point of the encoding and display process is that each shade in the source image is encoded into a type of SUSR pixel with a specific rotation angle θ. As shown in Fig. 4(d), we define four different shades in the picture to the SUSR pixels with four rotation angles 0°, 30°, 60°, and 90°. The SEM micrograph of the sample is shown in Fig. 4(e). The sample is 800 μm × 800 μm in size, and the incident light polarizes in the *x*-direction. With a FPA detector, we collect the reflection signal and integrate in 1200–1300 cm^{-1}. Figure 4(f) shows the decoded picture with four shades retrieved from the SUSR sample in Fig. 4(c). The brightness of the "bright" pixel is more than 10 times that of the "dark" pixel at the working frequency.

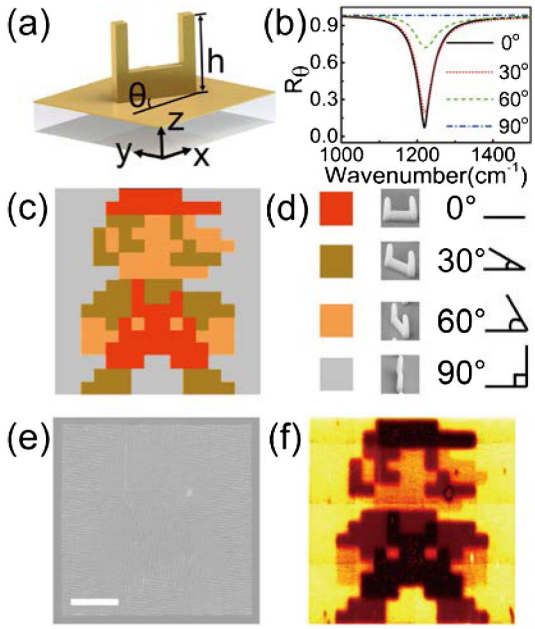

Fig. 4. (a) Schematic diagram of a rotated SUSR. $h = 1.9$ μm. θ represents the angle between the rim of the SUSR and x-axis. (b) Simulated reflection spectrum for different θ with the x-polarized incident light. (c) and (d) The picture is encoded into four regions where SUSR pixels have been rotated for $\theta = 0°$, 30°, 60°, and 90°, respectively. (e) SEM micrograph of the top view of the designed sample. The scale bar represents 200 μm. (f) FPA images by integrating in 1200–1300 cm^{-1}. The incident light is x-polarized.

In principle, we may encode a picture with higher resolution of grayscale level by dividing the rotation angle to smaller degrees. However, it should be pointed out that the relationship of the reflection intensity and the rotation angle θ is nonlinear. Around a certain angle (for example, around $\theta = \pi/4$) the reflection intensity is more sensitive to the angle rotation, whereas in some other regions (for example, around $\theta = 0$ or $\pi/2$), the intensity is not very sensitive to the angle rotation. Such a nonlinear relationship of the reflection intensity and the rotation angle θ limits the resolution of this grayscale display approach.

Encoding and display with multiple channel elements within an extremely limited space is an important topic in developing electro-optical display [24–26,33,34]. Here we experimentally demonstrate the polarization-dependent binary encoding and display by utilizing the resonant absorption and reflection of 3D microstructures. Although the fabrication of 3D microstructures is much more difficult, 3D structures have advantages for encoding and display, compared with 2D counterparts. For example, 3D structures may provide more degrees of freedom for encoding and display. Besides the arm height, we can also change the horizontal bar height of the SUSR structure to tune the absorption frequency [6]. It is feasible for us to use this feature to display different patterns at different frequencies. We also demonstrate the possibility to utilize the rotation angle of the SUSR to display an image with different grayscales. By introducing versatile 3D microstructures, we expect that our display approach may have promising applications in active display devices, information storage, and encryption technology.

Funding. National Natural Science Foundation of China (NSFC) (11474157, 11674155, 11574141, 11634005, 61475070); Natural Science Foundation of Jiangsu Province (BK20160065).

REFERENCES

1. J. M. Enoch, Optom. Vis. Sci. **83**, 775 (2006).
2. N. Yu and F. Capasso, Nat. Mater. **13**, 139 (2014).
3. A. Poddubny, I. Iorsh, P. Belov, and Y. Kivshar, Nat. Photonics **7**, 948 (2013).
4. M. Ozaki, J. Kato, and S. Kawata, Science **332**, 218 (2011).
5. N. Liu, M. Mesch, T. Weiss, M. Hentschel, and H. Giessen, Nano Lett. **10**, 2342 (2010).
6. X. Xiong, Z. H. Xue, C. Meng, S. C. Jiang, Y. H. Hu, R. W. Peng, and M. Wang, Phys. Rev. B **88**, 115105 (2013).
7. M. Born and E. Wolf, *Principles of Optics: Electromagnetic Theory of Propagation, Interference and Diffraction of Light*, 7th ed. (Cambridge University, 1999).
8. N. Yu, P. Genevet, M. A. Kats, F. Aieta, J. P. Tetienne, F. Capasso, and Z. Gaburro, Science **334**, 333 (2011).
9. X. J. Ni, N. K. Emani, A. V. Kildishev, A. Boltasseva, and V. M. Shalaev, Science **335**, 427 (2012).
10. A. V. Kildishev, A. Boltasseva, and V. M. Shalaev, Science **339**, 1232009 (2013).
11. A. A. High, R. C. Devlin, A. Dibos, M. Polking, D. S. Wild, J. Perczel, N. P. de Leon, M. D. Lukin, and H. Park, Nature **522**, 192 (2015).
12. G. Zheng, H. Muhlenbernd, M. Kenney, G. Li, T. Zentgraf, and S. Zhang, Nat. Nanotechnol. **10**, 308 (2015).
13. S. C. Jiang, X. Xiong, Y. S. Hu, S. W. Jiang, Y. H. Hu, D. H. Xu, R. W. Peng, and M. Wang, Phys. Rev. B **91**, 125421 (2015).
14. E. Karimi, S. A. Schulz, I. De Leon, H. Qassim, J. Upham, and R. W. Boyd, Light Sci. Appl. **3**, e167 (2014).
15. D. M. Lin, P. Y. Fan, E. Hasman, and M. L. Brongersma, Science **345**, 298 (2014).
16. T. W. Ebbesen, H. J. Lezec, H. F. Ghaemi, T. Thio, and P. A. Wolff, Nature **391**, 667 (1998).
17. H. T. Liu and P. Lalanne, Nature **452**, 728 (2008).
18. M. Kuwata-Gonokami, N. Saito, Y. Ino, M. Kauranen, K. Jefimovs, T. Vallius, J. Turunen, and Y. Svirko, Phys. Rev. Lett. **95**, 227401 (2005).
19. E. Plum, V. A. Fedotov, A. S. Schwanecke, N. I. Zheludev, and Y. Chen, Appl. Phys. Lett. **90**, 223113 (2007).
20. Y. Q. Ye and S. L. He, Appl. Phys. Lett. **96**, 203501 (2010).
21. N. I. Landy, S. Sajuyigbe, J. J. Mock, D. R. Smith, and W. J. Padilla, Phys. Rev. Lett. **100**, 207402 (2008).
22. N. Fang, H. Lee, C. Sun, and X. Zhang, Science **308**, 534 (2005).
23. J. B. Pendry, Phys. Rev. Lett. **85**, 3966 (2000).
24. T. Xu, Y. K. Wu, X. Luo, and L. J. Guo, Nat. Commun. **1**, 59 (2010).
25. E. Laux, C. Genet, T. Skauli, and T. W. Ebbesen, Nat. Photonics **2**, 161 (2008).
26. K. Kumar, H. Duan, R. S. Hegde, S. C. Koh, J. N. Wei, and J. K. Yang, Nat. Nanotechnol. **7**, 557 (2012).
27. J. K. Gansel, M. Thiel, M. S. Rill, M. Decker, K. Bade, V. Saile, G. von Freymann, S. Linden, and M. Wegener, Science **325**, 1513 (2009).
28. J. Valentine, S. Zhang, T. Zentgraf, E. Ulin-Avila, D. A. Genov, G. Bartal, and X. Zhang, Nature **455**, 376 (2008).
29. C. M. Soukoulis and M. Wegener, Nat. Photonics **5**, 523 (2011).
30. X. Xiong, Y. S. Hu, S. C. Jiang, Y. H. Hu, R. H. Fan, G. B. Ma, D. J. Shu, R. W. Peng, and M. Wang, Appl. Phys. Lett. **105**, 201105 (2014).
31. N. Liu, H. C. Guo, L. W. Fu, S. Kaiser, H. Schweizer, and H. Giessen, Nat. Mater. **7**, 31 (2007).
32. G. Dolling, C. Enkrich, M. Wegener, C. M. Soukoulis, and S. Linden, Science **312**, 892 (2006).
33. L. Wang, T. Li, R. Y. Guo, W. Xia, X. G. Xu, and S. N. Zhu, Sci. Rep. **3**, 2603 (2013).
34. Z. M. Yang, Y. M. Zhou, Y. Q. Chen, Y. S. Wang, P. Dai, Z. G. Zhang, and H. G. Duan, Adv. Opt. Mater. **4**, 1196 (2016).